Exciton properties and optical response in $In_xGa_{1-x}As/GaAs$ strained quantum wells

R. Atanasov and F. Bassani
Scuola Normale Superiore, Piazza dei Cavalieri 7, I-56126 Pisa, Italy

A. D'Andrea and N. Tomassini
Istituto Metodologie Avanzate Inorganiche, Consiglio Nazionale delle Ricerche, Monterotondo Stazione, I-00016 Roma, Italy
(Received 13 April 1994; revised manuscript received 21 July 1994)

Exciton binding energies and optical response in quantum wells and in multiple quantum wells of $GaAs/In_xGa_{1-x}As/GaAs$ are computed by a variational envelope-function procedure using the four-band model and the simpler two-band model. The effect of hydrostatic and uniaxial strain are considered from a virtual-crystal stress Hamiltonian. The physical parameters used for the alloy ($In_xGa_{1-x}As$) are obtained by interpolating the parameter values of pure materials (GaAs, InAs). We verify that band-offset values in the range of 0.30–0.45 give exciton states and optical response in good agreement with experiments. The light-hole exciton energy is also well reproduced by theory and results are very close to the continuum states of the well, its binding energy being due to the attraction of the electron, localized inside the well.

I. INTRODUCTION

Pseudomorphic epitaxial layers grown on a bulk substrate have attracted great interest because lattice strain can be considered an additional parameter for tailoring the optoelectronic properties of nanoscale devices. In the last five years, pseudomorphic $In_xGa_{1-x}As/GaAs$ heterostructures have been intensively studied[1–9] and their physical properties have been shown to be related to exciton localization and strain effect. Some points are still open, such as the confinement properties of the light-hole exciton[5] (first or second kind of exciton), the plastic phase observed in large quantum wells[10,11] (in which range of dimensions this phase is stable with respect to the strained and dislocated phases), and finally the valence-band-offset value (different values in different samples are reported in the literature[2–6]).

All these open questions have prompted us to undertake a systematic study of excitons and optical properties in these materials without using fitting parameters. This study is also relevant for the theoretical evaluation of new phenomena, like second harmonic generation in asymmetric quantum wells, exciton localization in the barriers, etc. The aim of the present paper is twofold, namely, (a) to infer from interpolated known bulk values the relevant features of quantum well excitons necessary to reproduce a large number of experimental results recently appearing in the literature, and (b) to study the light-hole exciton in $In_xGa_{1-x}As/GaAs$ quantum wells, in the absence of hole confinement.

It is well known that excitons in $In_xGa_{1-x}As/GaAs$ confined systems can be described in the effective mass approximation by a 3×3 matrix Hamiltonian which includes the Luttinger Hamiltonian[12] and the internal strain Hamiltonian[13–15] for the valence band, and a spherical effective mass Hamiltonian for the conduction band, as well as the finite confinement potentials. The basic new idea of this paper is to account for the strain effects in the exciton Hamiltonian, by using a virtual-crystal model for the strain.

In Sec. II, this 3×3 matrix Hamiltonian is solved variationally by an envelope trial function expanded in electron-hole subband products. Since the light-hole energy is very close to the continuum of states,[7] a quasi-continuum of electron and hole states is adopted with a confinement box. In Section III we compute exciton polarizability and absorption spectra, solving Maxwell equations and taking into account spatial dispersion effects for single wells and for multiple quantum wells. In order to have a simpler exciton model and to include intersubband contributions a simplified two-band model is also introduced for strained materials. The calculated absorption spectra compare well with experimental data. In Sec. IV numerical results for a large set of samples are obtained. Our model is able to reproduce resonant energies of heavy- and light-hole excitons, as given experimentally. Conclusions are given in Sec. V.

II. EXCITON PROPERTIES

It is well known that the large lattice mismatch between GaAs (a_0=5.654 Å) and InAs (a_0=6.06 Å) leads to biaxial compression strain when an alloy of $In_xGa_{1-x}As$ is grown on the (001) surface of a GaAs substrate. This can be decomposed into a uniaxial and a hydrostatic component. The uniaxial deformation potential removes the degeneracy between heavy- and light-hole bands at the Γ point, and the hydrostatic component rigidly shifts the band gap energies.

Let us consider a multiple quantum well of $In_xGa_{1-x}As/GaAs$ grown along the [001] crystallographic direction, which we take as the z axis of our frame of reference. The exciton Hamiltonian may by written as

a 3×3 matrix,

$$\boldsymbol{H}_{\rm ex} = \boldsymbol{T}_v(-i\nabla_{z_h}) - \boldsymbol{S}_v + [T_c(-i\nabla_{z_e}) + S_c + E_g(x) + V_{\rm Coul}(|\boldsymbol{r}_e - \boldsymbol{r}_h|) + V_{\rm im}(\boldsymbol{r}_e, \boldsymbol{r}_h)]\boldsymbol{I}. \quad (1)$$

In the above expression $\boldsymbol{T}_v$ is the valence 3×3 Luttinger Hamiltonian matrix,[12] and $\boldsymbol{S}_v$ is the strain matrix of the valence band. Analogously, T_c is the electron kinetic energy in the conduction band, S_c is the corresponding hydrostatic energy, and $E_g(x)$ is the unstrained alloy band gap inside the quantum well (QW), which for $x = 0$ becomes the GaAs band gap. The electron-hole potential is given by a Coulomb term $V_{\rm Coul}$, and an image charge contribution $V_{\rm im}$, produced by the dielectric function mismatch. In order to preserve the matrix dimensionality in Eq. (1), the terms in square brackets are multiplied by the unitary 3×3 matrix $\boldsymbol{I}$.

We compute the exciton envelope functions as a linear combinations of the electron and hole subband products. These subbands are the eigenstates of the Hamiltonian (1) when the electron-hole interaction is neglected.

A. Electron and hole states

We must first of all compute the electron and hole states, and consider the influence on them of the strain potential due to the lattice mismatch. This is done by adding a strain contribution to the usual confining potential due to the different band gaps.

The usual confining potential is the same as in the lattice matched QW's, and is given by the difference in band gaps ΔE_g, subdivided between electron and hole states according to a universal factor $Q_v^{\rm LM}$, which is expressed as a ratio between the shift ΔE_v of the fourfold degenerate Γ_8 valence band and the band gap shift ΔE_g. We will show that the exciton binding energy is not strongly dependent on $Q_v^{\rm LM}$, and will choose a value Q_v which accounts also for the strain.

The lattice mismatch introduces an additional term in the confining potential, which is known in perfect crystals. Using the virtual-crystal model we introduce this term as an x-dependent interpolated potential, related to the parameter

$$\delta_L(x) = a_0(0)/a_0(x) - 1, \quad (2)$$

where $a_0(x)$ is the lattice parameter of the alloy.

The strain potential for the conduction band is[13–15]

$$S_c = a_c(\varepsilon_{xx} + \varepsilon_{yy} + \varepsilon_{zz}), \quad (3)$$

with strain components given by

$$\varepsilon_{xx} = \varepsilon_{yy} = \delta_L,\ \varepsilon_{zz} = -2\delta_L C_{12}/C_{11}. \quad (4)$$

Here, $\hat{\varepsilon}$ is the strain tensor, a_c is the hydrostatic deformation potential of the conduction band, and C_{11} and C_{12} are the elastic stiffness constants.

For the valence band, we can write the strain Hamiltonian as[13–15]

$$\boldsymbol{S}_v = -\begin{bmatrix} \delta E_H - \delta E_S & 0 & 0 \\ 0 & \delta E_H + \delta E_S & \sqrt{2}\delta E_S \\ 0 & \sqrt{2}\delta E_S & \Delta_0 + \delta E_H \end{bmatrix}, \quad (5)$$

where the hydrostatic (δE_H) and the shear (δE_S) energies are given by

$$\delta E_H = a_1(\varepsilon_{xx} + \varepsilon_{yy} + \varepsilon_{zz}),\quad \delta E_S = b_1(\varepsilon_{xx} - \varepsilon_{zz}). \quad (6)$$

The strain by itself removes the fourfold degeneracy of Γ_8 splitting it into heavy-hole (hh) and light-hole (lh) states, separated by $2\delta E_s$, and shifts the split-off (SO) band. The hydrostatic component shifts rigidly all valence states by δE_H, and the conduction states by S_c. Consequently, we can fully account for the stress effect and band mismatch by introducing three different band gaps $E_{gS}^{\beta}(x)$ (β =hh, lh, SO) between the conduction band and the corresponding β valence band inside the quantum well. They result in the following expressions:

$$\begin{aligned} E_{gS}^{\rm hh} &= E_g(x) + \delta E_H - \delta E_S, \\ E_{gS}^{\rm lh} &= E_{gS}^{\rm hh} + 2\delta E_S \\ &\quad + \frac{1}{2}[\Delta_0 - \delta E_S - \sqrt{(\Delta_0 - \delta E_S)^2 + 8\delta E_S^2}], \\ E_{gS}^{\rm SO} &= E_{gS}^{\rm lh} + \sqrt{(\Delta_0 - \delta E_S)^2 + 8\delta E_S^2}, \end{aligned} \quad (7)$$

where Δ_0 is the unstrained split-off energy, and the strain energies are given by

$$\begin{aligned} \delta E_H(x) &= 2a(1 - C_{12}/C_{11})\delta_L\ , \\ \delta E_S(x) &= b(1 + 2C_{12}/C_{11})\delta_L, \end{aligned} \quad (8)$$

where $a(x)$ ($a = a_c - a_1$) and $b(x)$ ($b = b_1$) are the alloy deformation potentials. The above gaps imply different confinement potentials for the electron (V_e) and for the holes (V_β), which are determined from the band-offset parameter $Q_v^{\rm LM}$. On the other hand, in the case of strained $Ga_{1-x}In_xAs/GaAs$ quantum wells both δE_H and δE_S are positive quantities, and hence the fundamental band gap in the well region $E_{gS}(x)$ coincides with $E_{gS}^{\rm hh}$. This means that the experimentally measured valence band offset Q_v is given by $Q_v = |\Delta E_{\rm hh}|/[E_g(0) - E_{gS}] \equiv V_{\rm hh}/(V_{\rm hh} + V_e)$, where $V_e, V_\beta > 0$. The knowledge of Q_v together with Eqs. (8) determines the electron $[V_e(z)]$ and hole $[V_\beta(z)]$ quantum well shapes.

In the present work, the parameters of the $In_xGa_{1-x}As$ alloy are obtained by a linear interpolation of the corresponding bulk values given in Table I; for the band gap and the split-off energies at temperature $T = 2$ K we adopt the following expressions:[16]

$$\begin{aligned} E_g(x) &= E_g(0) - 1.5837x + 0.475x^2\ , \\ \Delta_0(x) &= \Delta(0) - 0.09x + 0.14x^2. \end{aligned} \quad (9)$$

The strained gaps can then be found for all alloy concentrations. We report in Fig. 1 the confinement potentials, with a value of Q_v=0.45. We observe that V_e and $V_{\rm hh}$ are much greater than $V_{\rm lh}$, and in the range of indium concentrations adopted (x=0.05–0.3), the light hole is not confined. To investigate the role of the band offset we have performed our further calculations with two

TABLE I. Parameter values adopted in the exciton calculations (from Ref. 21).

	GaAs	InAs
a_0 (Å)	5.6533	6.0584
C_{11} (dyn/cm^2)	11.88 10^a	8.33 10^a
C_{12} (dyn/cm^2)	5.38 10^a	4.30 10^a
a (eV)	-9.8	-5.8
b (eV)	-1.7	-1.8
γ_1	6.85	19.67
γ_2	2.10	8.37
ε_b	12.5	14.6
E_g (eV)	1.5192	0.4105
Δ_0 (eV)	0.341	0.391

[a]From Ref. 11.

different values of the offset parameter, $Q_v = 0.30$ and $Q_v = 0.45$. These values are chosen among those suggested in the recent literature,[1–9] and we adopt them without further justification. The energy is conventionally referred to the top of the heavy-hole subband inside the well, taking the strain into account.

B. Four-band exciton model

Let us consider the exciton envelope function Ψ^β expanded in the form

$$\Psi^\beta(r, z_e, z_h) = \sum_{i,j,\beta'} C_{ij}^{\beta\beta'} u_i(z_e) u_j^{\beta'}(z_h) F_{ij}^\beta(r) \ , \qquad \beta = \text{hh, lh, SO}, \quad (10)$$

where $F_{ij}^\beta(r)$ denotes the exciton amplitude, $r = \sqrt{\rho^2 + z^2}$, $\boldsymbol{\rho} = (x, y)$ is the in-plane two-dimensional vector, and $u_i(z_e)$ and $u_j^\beta(z_h)$ are the electron and β-hole envelope functions, respectively. In this representation we choose the coefficients $C_{ij}^{\beta\beta'}$ to diagonalize the total exciton Hamiltonian (1), which can be written in the form

$$\boldsymbol{H}^{\text{ex}} = \begin{bmatrix} H_{\text{hh}} & 0 & 0 \\ 0 & H_{\text{lh}} & H_{\text{lh-SO}} \\ 0 & H_{\text{SO-lh}} & H_{\text{SO}} \end{bmatrix} . \quad (11)$$

Here, the diagonal matrix elements are given by

$$H_\beta^{\text{ex}} = -\frac{\hbar^2}{2\mu_\beta} \nabla_{\boldsymbol{\rho}}^2 + H_c(z_e) + H_\beta(z_h) + V_{\text{coul}}(|\boldsymbol{r}_e - \boldsymbol{r}_h|) + V_{\text{im}}(\boldsymbol{r}_e, \boldsymbol{r}_h), \quad (12)$$

where μ_β denotes the in-plane electron β-hole reduced mass, H_β is the hole-confining Hamiltonian in the z direction,

$$H_\beta(z_h) = -\frac{\hbar^2}{2} \frac{\partial}{\partial z_h} \frac{1}{m_\beta} \frac{\partial}{\partial z_h} + V_\beta(z_h), \quad (13)$$

and similarly for the electron-confining Hamiltonian H_c. The hole effective masses in the z direction m_β as well as the corresponding in-plane masses $m_{\|\beta}$ are related to the Luttinger parameters by the relations

$$m_{\text{hh/lh}} = \frac{m_0}{\gamma_1 \mp 2\gamma_2} \ , \ m_{\|\text{hh/lh}} = \frac{m_0}{\gamma_1 \pm \gamma_2} \ , \ m_{\text{SO}} = \frac{m_0}{\gamma_1}. \quad (14)$$

The off-diagonal elements in Eq. (11) provide the lh-SO exciton interaction

$$H_{\text{lh-SO}} = H_{\text{SO-lh}} = \frac{\hbar^2}{\sqrt{2}} \frac{\partial}{\partial z_h} \left(\frac{1}{m_{\text{lh}}} - \frac{1}{m_{\text{SO}}} \right) \frac{\partial}{\partial z_h}. \quad (15)$$

The electron (E_i) and hole (E_j^β) energies produced by quantum confinement and the corresponding envelope functions are obtained as solutions of the following equations:

$$H_c u_i = E_i u_i, \ H_\beta u_j^\beta = E_{j\beta} u_j^\beta, \qquad i, j = 1, 2, \ldots, \beta = \text{hh, lh, SO}, \quad (16)$$

where the matching conditions on the well-barrier surfaces consist in the continuity of the wave envelope functions and the conservation of the current.[17,18] In order to obtain discrete numerable states also in the continuum, we consider our system of single or multiple quantum well to be placed inside a large one-dimensional box of thickness L_{box} and apply the so-called "no-escape boundary conditions"[19,20] given by

$$u_i(\pm L_{\text{box}}/2) = u_j^\beta(\pm L_{\text{box}}/2) = 0. \quad (17)$$

We calculate the exciton states in a system of single or multiple QW by means of a variational procedure, which is carried out in two steps. First, we take the exciton amplitudes $F_{ij}^\beta(r)$ in the form of a three dimensional $1s$-

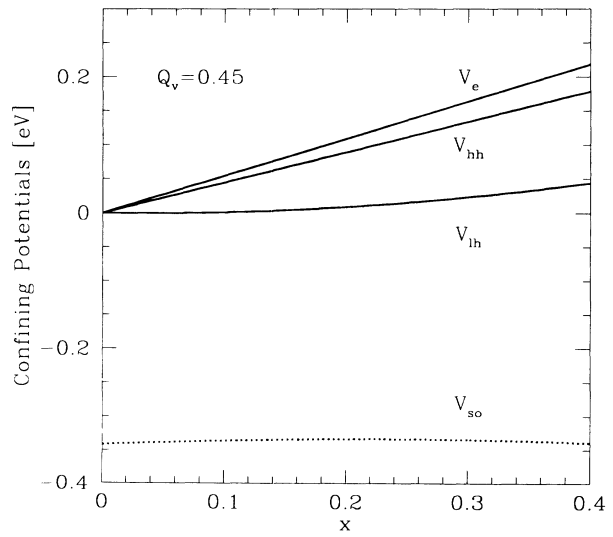

FIG. 1. Electron (V_e) and hole (V_β; β =hh,lh,SO) confinement potentials as functions of the indium concentration x in an $In_xGa_{1-x}As$ quantum well, where the valence band offset is Q_v=0.45. Strain effects are included.

like wave function

$$F_{ij}^{\beta}(r) = \exp(-r/\lambda_{ij}^{\beta}), \tag{18}$$

where the effective exciton radious λ_{ij}^{β} is obtained by minimization of the $H_{\beta}^{\rm ex}$ matrix element. The second step consists in diagonalizing $\boldsymbol{H}^{\rm ex}$ in the basis Ψ^{β} with the appropriate boundary conditions. Thus we obtain a set of exciton energies E^{ν} and the corresponding envelope functions $\Psi^{\nu\beta}$, which are classified by the quantum number ν ($\nu = 1, 2, ...$). In Table II we show results for the lowest exciton binding energies R^1 in a variety of quantum wells, and compare them with available experimental data.

C. Two-band exciton model

In this section we use two decoupled Hamiltonians $H_{\rm hh}^{\rm ex}$ and $H_{\rm lh}^{\rm ex}$ to calculate the heavy-hole and light-hole excitons, respectively. The effect of the split-off band is included into the band effective masses and the conduction–light-hole band gap $E_{\rm gS}^{\rm lh}$. We calculate the alloy electron $m_e(x)$ and hole $m_{\beta}(x)$ effective masses along the z direction by a linear interpolation of the corresponding values in bulk[4,16] GaAs ($x = 0$) and InAs ($x = 1$) and obtain

$$m_e = 0.067 - 0.044x \ , \quad m_{\rm lh} = 0.08 - 0.04x \ , \qquad m_{\rm hh} = 0.454 - 0.044x. \tag{19}$$

All the in-plane reduced electron-hole masses μ_{β} are calculated as explained in Ref. 22 by relating them to the Luttinger parameters [as shown in expression (14)]. The other physical parameters used in the calculations are the same as adopted in the four-band model and reported in Table I.

(a) *Heavy-hole excitons.* The two-band Hamiltonian $H_{\rm hh}^{\rm ex}$ is given by Eq. (12), and the masses m_e, $m_{\rm hh}$, and $\mu_{\rm hh}$ are calculated as shown above. Then, we consider exciton states $\Psi_{ij}^{\rm hh}$ attached to the ith electron and the jth heavy-hole subband. The exciton envelope function is taken as a quasi-two-dimensional $1s$-like function of the form

$$\Psi_{ij}^{\rm hh}(\rho, z_e, z_{\rm hh}) = u_i(z_e) u_j^{\rm hh}(z_{\rm hh}) F_{ij}^{\rm hh}(\rho), \tag{20}$$

where u_i and $u_j^{\rm hh}$ are the solutions of Eq. (16), and the $1s$-exciton amplitude is $F_{ij}^{\rm hh}(\rho) = \sqrt{2/\pi}\exp(-\rho/\lambda_{ij})/\lambda_{ij}$, with a similar expression for the $2s$ exciton.[22,23] The effective exciton radius λ_{ij} is determined by a variational procedure as in the previous section, minimizing the exciton energy $E_{ij}^{\rm hh}$. Results for the same QW's previously treated with the four-band model are given in Table II. We can observe that in the thickness range where strong confinement occurs the results obtained with the two-band model agree fairly well with those of the four-band model and with experiments, thus justifying the use of this simple model.

In the case of subband levels very close in energy (e.g., QW's with large L_w) the two-band approximation is not sufficient to give the precise exciton energy, and we may improve the model by considering interaction between subbands. The exciton envelope function is

$$\Psi^{\rm hh}(\rho, z_e, z_h) = \sum_{i,j} C_{ij}^{\rm hh} u_i(z_e) u_j^{\rm hh}(z_h) F_{ij\,\rm hh}(\rho), \tag{21}$$

and the exciton energies $E^{\nu\,\rm hh}$ are determined by diagonalization of $H_{\rm hh}$. Results from this second step in the calculation of the first heavy-hole exciton state $\Psi^{\rm 1hh}$ are given in the last column of Table II.

(b) *Light-hole excitons: Confinement from electron localization.* In widely used lattice matched QW's (e.g., GaAs/$Ga_{(1-x)}Al_xAs$), the above described two-band model gives good results also for light-hole exciton states.[22] The main approximation in these models is to neglect the small off-diagonal elements $H_{\text{lh-so}}$ in Eq. (11). In the present case of strained QW's, the light-hole band always interacts with the split-off band because the uniaxial strain component E_S gives a nonzero component $S_{\text{lh-so}}$ in the strain Hamiltonian (5). In the present two-band approach, the strain effect influences the light-hole band gap $E_{\rm gS}^{\rm lh}$, according to Eq. (8). It yields a small rigid shift of the exciton position toward the lower energies. Another feature of the light-hole states is that, because of the strain, they are not confined by the well potential $V_{\rm lh}$ alone. For this reason the light-hole qua-

TABLE II. Binding energies R of the lowest heavy-hole exciton for a large number of quantum wells, where experimental results are available. In the fourth, fifth, and sixth columns we report theoretical results computed by four-band (FB), two-band (TB), and mixed two-band (MTB) models. All energies are given in meV.

x	L_w (nm)	R expt.	R^1 FB	$R_{11}^{\rm hh}$ TB	$R^{\rm 1hh}$ MTB
0.05	7.2	7.4[a]	7.18	6.9	7.4
0.05	10.2	7.4[a]	6.81	6.8	7.8
0.05	14.2	7.4[a]	6.53	6.5	7.5
0.05	16.4	7.0[a]	6.37	6.3	7.6
0.05	18.4	6.1[a]	6.19	6.1	7.5
0.10	8.0	7.45[b]	6.98	7.4	8.2
0.13	10.7	7.0[c]	6.80	7.19	8.3
0.13	15.0	6.6[c]	6.38	6.65	8.1
0.135	1.0	4.2[c]	4.67	5.6	5.6
0.135	2.0	7.0[c]	6.99	7.1	7.1
0.135	3.0	7.8[c]	7.32	7.68	7.68
0.15	1.4	6.5[d]	6.26	6.6	6.6
0.15	2.5	8.8[d]	7.88	7.7	7.7
0.15	4.8	9.2[d]	7.99	8.1	8.7
0.22	5.0	9.0[c]	7.83	8.1	8.5
0.22	7.5	8.3[c]	7.50	7.7	8.4

[a]M. J. Joyes, Superlatt. Microstruct. **12**, 293 (1992).
[b]H. Hou, Y. Segawa, Y. Aoyagi, S. Namba, and J. Zhou, Phys. Rev. B **42**, 1284 (1990).
[c]J. Reithmaier, R. Hoger, and H. Riechert, Phys. Rev. B **43**, 4933 (1991).
[d]K. Moore, G. Duggan, K. Woodbridge, and C. Roberts, Phys. Rev. B **41**, 1090 (1990).

sicontinuum $u_j^{\rm lh}$ is used, as determined by the no-escape boundary conditions of Eq. (17) and the contribution of the well potential. Consequently, the main potential confining the light hole is the Coulomb potential of the electron, which is well localized inside the QW. As discussed for impurity acceptors[24] the convergence in the expansion of the exciton function in the quasicontinuum states is enormously improved when the confinement box is chosen to have an appropriate length. We use this fact to consider the box length $l_{\rm box}$ as a second variational parameter. In this way, we perform a minimization of the exciton energy

$$E_{ij}^{\rm lh}[l_w,\lambda_{ij\rm lh}]=\langle u_i u_j^{\rm lh}F_{ij\rm lh}|H_{\rm lh}|F_{ij\rm lh}u_j^{\rm lh}u_i\rangle \tag{22}$$

with respect to the exciton radius and to $l_{\rm box}$. The resulting $l_{\rm box}$ may be interpreted as the length along the z axis where the light hole is confined due to the electron Coulomb field. Further improvement in the calculation of $E_{ij}^{\rm lh}$ may be obtained by including more than one quasicontinuum state; however in the interesting range of QW widths, where the exciton states are well confined, this procedure yields small corrections to $E_{ij}^{\rm lh}$, as well as to the corresponding oscillator strengths. Thus, the above presented variational method gives a possibility to classify the exciton states by the corresponding subband indices $(ij\beta)$, as well as to discuss the optical properties of QW's in terms of heavy-hole and light-hole excitons separately.

III. OPTICAL RESPONSE OF EXCITONS IN MULTIPLE QUANTUM WELLS

We now consider the problem of computing the optical properties, and to be close to the experimental situation, we consider the case of multiple QW's. The Maxwell equation for an electromagnetic wave at normal incidence on the QW plane to be solved is

$$\nabla_z^2\boldsymbol{E}(z)+\frac{\omega^2\varepsilon_b(z)}{c^2}\boldsymbol{E}(z)+\frac{\omega^2}{c^2}\boldsymbol{P}_{\rm ex}(z)=0, \tag{23}$$

where $\boldsymbol{P}_{\rm ex}$ is the exciton polarization, and the steplike function $\varepsilon_b(z)$ takes the value ε_B in the barrier and ε_b in the well. We express the exciton polarization by means of the exciton energies E^ν and the corresponding envelope functions $\Psi^{\nu\beta}$ as given by Eq. (10) and obtain

$$\begin{aligned}\boldsymbol{P}_{\rm ex}(\omega,z)&=\int\chi_{\rm ex}(\omega,z,z')\boldsymbol{E}(z')dz'\\&=\sum_{\nu\beta\beta'}S^\nu(\omega)\tilde\Psi^{\nu\beta}\boldsymbol{I}^{\nu,\beta'}(\omega),\end{aligned} \tag{24}$$

where the resonant part

$$S^\nu(\omega)=\frac{S_0}{\hbar\omega-E^\nu-i\Gamma^\nu}\ ,\quad S_0=e^2E_K/4\pi m_0\omega^2, \tag{25}$$

has been separated from the spatial contribution

$$\tilde\Psi^{\nu\beta}(z)=\sum_{i,j,\beta'}c_{\beta'}C_{ij}^{\beta\beta'}u_i(z)u_j^{\beta'}(z)F_{ij}^{\beta'}(0), \tag{26}$$

where the coefficients $c_{x\beta}$ are related to the Kane energy E_K, the momentum matrix elements in the bulk $|\langle c|P_x|\beta\rangle|^2=c_{x\beta}^2E_Km_0/2$, and $c_{x\rm hh}=1/\sqrt{2}$, $c_{x\rm lh}=1/\sqrt{6}$, and $c_{x\rm SO}=1/\sqrt{3}$. The integral $\boldsymbol{I}^{\nu\beta}$ accounts for the nonlocal character of the optical response and is expressed by

$$\boldsymbol{I}^{\nu\beta}(\omega)=\sum_J\int_J dz\,[\tilde\Psi^{\nu\beta}(z)]^*\boldsymbol{E}_J(\omega,z). \tag{27}$$

In the above equation, the subscript J labels the different regions in the sample (barrier, well, substrate, etc.) and the integration on z is performed in the corresponding region.

We solve Eq. (23) in two steps: (1) we determine the electric field in each Jth region of the multiple QW introducing two plane waves of opposite direction with arbitrary amplitudes $\boldsymbol{A}_J$ and $\boldsymbol{B}_J$, and (2) we match the electric fields at each interface and solve exactly the Maxwell equation as in Ref. 19. Thus, the electric field inside the Jth region is given in the form

$$\boldsymbol{E}_J(z)=\boldsymbol{A}_J\exp(iq_Jz)+\boldsymbol{B}_J\exp(-iq_Jz)+\boldsymbol{E}_J^0(z), \tag{28}$$

where the wave vector $q_J=\omega\sqrt{\varepsilon_J}/c$, and ε_J is the value of $\varepsilon_b(z)$ inside the region under consideration. The field E_J^0 is a particular solution of Eq. (23) and gives

$$\begin{aligned}\boldsymbol{E}_J^0(z)=\frac{-i}{2q_J}\int_{z_J^0}^z dz'\{&\exp[iq_J(z-z')]\\&-\exp[-iq_J(z-z')]\}\boldsymbol{F}_J(z'),\end{aligned} \tag{29}$$

where z_J^0 is the begining of the Jth region, and

$$\boldsymbol{F}_J(z)=-\frac{\omega^2}{c^2}\sum_\nu S_\nu\tilde\Psi^{\nu\beta}\boldsymbol{I}^{\nu\beta}. \tag{30}$$

We apply the operator $\int dz\tilde\Psi^{\nu\beta}$ to Eq. (28) and summing on J obtain a linear system of equations for the unknown coefficients $\boldsymbol{I}^{\nu\beta}$. The amplitudes A_J and B_J are determined by the boundary conditions on the interfaces, involving $\boldsymbol{E}_J^0$ given by Eq. (28).

Then, we calculate the reflectivity r and transmission t coefficients of the sample, and the absorbance A. The absorbance A is given by

$$A=\exp(-\alpha L_T)-1=(1-|r|^2-|t|^2)/(1-|r|^2), \tag{31}$$

where α is the absorption coefficient, and L_T is the total length of the sample. We show in Fig. 2 the results for a typical multiple QW, computed from the four-band model of the previous section; the experimental data[7] for the same sample are also reported. The nonradiative linewidths Γ^ν to be inserted in Eq. (25) are taken to be $\Gamma^{\rm hh}=0.8$ meV and $\Gamma^{\rm lh}=0.7$ meV. The total dampings Γ^β which result from our calculation are very close to those given by the experiment;[7] $\Gamma^{\rm hh}=1.4$ meV and $\Gamma^{\rm lh}=0.8$ meV. We also see from Fig. 2 that the theoretical spectra are in good agreement in their exciton positions and oscillator strengths.

In order to give a simpler interpretation of the absorption spectra which also takes into account the continuum

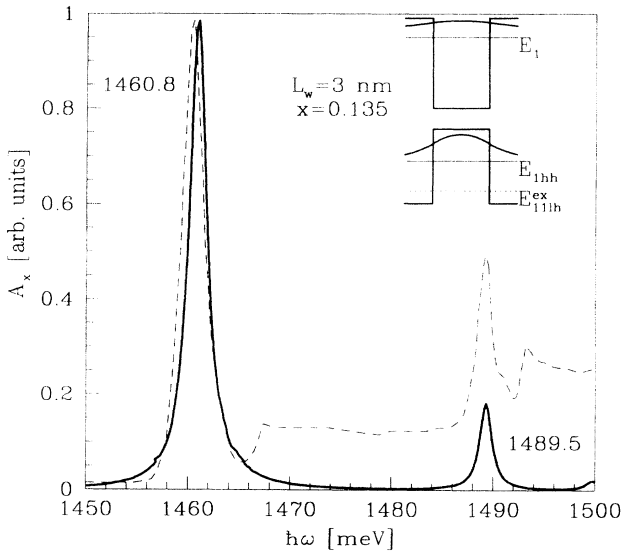

FIG. 2. Exciton absoption spectra of an $In_xGa_{1-x}As/GaAs$ multiple QW with $L_w = 3$ nm, $x = 0.135$, and a barrier region of length 60 nm. The solid line shows the exciton spectrum calculated for the four-band theoretical model; the dashed line reproduces the experimental absorption (Ref. 7) in the same sample. The energy levels and some electron and hole states are given in the inset, where the light-hole exciton level is also indicated. The value of the band mismatch is $Q_v = 0.30$.

contribution, we calculate the absorption coefficient α by means of the two-band model described in the previous section. As shown in Ref. 23, α is proportional to the imaginary part of an averaged QW dielectric function and may be written in the form

$$\alpha_p(\omega) = \sum_{ij\beta} \left[\alpha_p^{\mathrm{ex}}(i,j,\beta,\omega) + \alpha_p^{\mathrm{el}}(i,j,\beta,\omega)\right] \langle u_i | u_j^{\beta}\rangle^2, \tag{32}$$

where the index p ($p = x, y, z$) refers to the polarization of the electric field, α_p^{ex} gives the contribution of the bound exciton states, and α_p^{el} is the contribution of the free electron-hole pairs (continuum). Expressing the exciton matrix elements in terms of the Kane energy as shown before, we obtain the exciton contribution, which given in the electric-dipole presentation has the form

$$\alpha_p^{\mathrm{ex}}(i,j,\beta,\omega) = \frac{8e^2 E_K c_{p\beta}^2 \hbar^3 \omega^2}{\sqrt{\varepsilon_B}\varepsilon_0 c\pi (L_w + L_B) m_0 \lambda_{ij}^{\beta\,2}} \times \sum_{n=1,2} \frac{\Gamma_{ij}^{\mathrm{ex}}\, 27^{1-n} / E_{ij}^{\beta(n)}}{[E_{ij}^{\beta(n)\,2} - (\hbar\omega)^2]^2 + 4(\hbar\omega)^2 \Gamma_{ij}^{\mathrm{ex}\,2}}, \tag{33}$$

and the continuum contribution

$$\alpha_p^{\mathrm{el}}(i,j,\beta,\omega) = \frac{2e^2 E_K c_{p\beta}^2 \mu_\beta \hbar\omega^2}{\sqrt{\varepsilon_B}\varepsilon_0 c\pi (L_w + L_B) m_0} \times \int d\epsilon \frac{\Gamma_{ij}^{\mathrm{el}}\, C(\epsilon)/E_{ij}^{\beta}(\epsilon)}{[E_{ij}^{\beta\,2}(\epsilon) - (\hbar\omega)^2]^2 + 4(\hbar\omega)^2 \Gamma_{ij}^{\mathrm{el}\,2}}. \tag{34}$$

Here the index n labels the exciton $1s$ ($n = 1$) and $2s$ ($n = 2$) bound states, $C(\epsilon)$ is the Coulomb enhancement factor,[23] and the coefficient $c_{z\mathrm{hh}} = 0$, $c_{z\mathrm{lh}} = \sqrt{2/3}$, and the other $c_{x\beta}$ coefficients are the same as in Eq. (25).

We show in Fig. 3 the absorption spectrum of various polarizations for the same sample considered in Fig. 2. We can observe the remarkable agreement between theoretical and experimental line shapes and peak positions, taking into consideration the fact that no adjustable parameters have been used. We see that the $2s$ states have a very small intensity in comparison with the $1s$ excitons and the continuum. Also the continuum absorption is in a fair agreement with the experiment, but the light-hole continuum is relatively weaker just near the edge. That could be explained by a strain enhancement of the in-plane masses and bulk matrix elements. The relative shift of the lh exciton peak towards higher energies is related to the choice of m_{lh} and to the lh-SO interaction.

IV. CALCULATIONS ON DIFFERENT SAMPLES

Calculations are performed both in the four-band model and in the two-band model for a large number

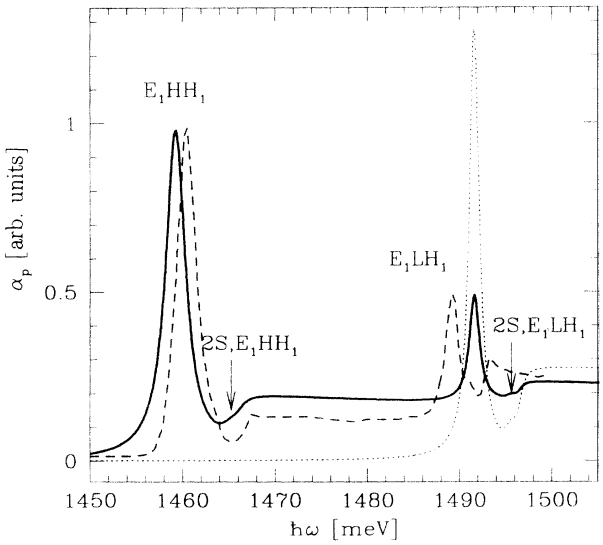

FIG. 3. Absorption spectra of the same QW sample as in Fig. 2, calculated by the two-band exciton model. The solid line gives the absorption coefficient α_x for an in-plane polarized electromagnetic wave ($p = x, y$), and the dotted line presents the corresponding spectrum when the electric field is polarized in the z direction (α_z). The interband contribution is also given in this model. The dashed line gives the experimental spectrum (Ref. 7). The value of the band mismatch is $Q_v = 0.45$.

of samples reported in the literature, with indium concentrations that range from 5% to 22% and making use of two different valence band offsets, $Q_v = 0.45$ and $Q_v = 0.30$. The purpose is to better clarify the accuracy of the two models and to decide on the role of the valence band offset Q_v, besides investigating the range of validity of the virtual-crystal method for the strain calculation. We observe from the results of Table II that the exciton binding energies computed by the four-band model are contained in the range of ± 0.5 meV with respect to the experimental values and only for two samples is the discrepancy greater than 1 meV. We obtain good agreement also using the two-band model, while the interaction between subbands is required only for very large wells and very small indium concentration, as expected from the fact that the cylindrical symmetry is less relevant in these cases.

To first investigate the role of the band offset we have carried out a systematic analysis of samples at 5% indium concentration with the four-band model, and both band-offset values. The computed exciton binding energies as functions of the well width are reported in Fig. 4, where the experimental results are also given. We have chosen the four-band model because for large wells and small barriers the two-band approximation is less accurate. By comparing the theoretical curves with the experimental values as functions of well thicknesses we can confirm the goodness of the interpolation scheme adopted for determining the alloy parameter values. In Fig. 5 exciton binding energies as functions of well thickness are given for samples with larger indium concentration ($x = 0.135$) with the two-band and the four-band model; we choose $Q_v = 0.45$, since the difference in Q_v is not significant, as shown also in Fig. 4. The agreement between theory and experiment is excellent if we consider only the samples of Ref. 7; in fact we reproduce the exciton binding energy in the whole range of quasi-two-dimensional transition.[7] The samples of Ref. 3 are shifted by ~ 0.5 meV, and the systematic energy difference reported in Fig. 5 between our calculations and the experimental results can

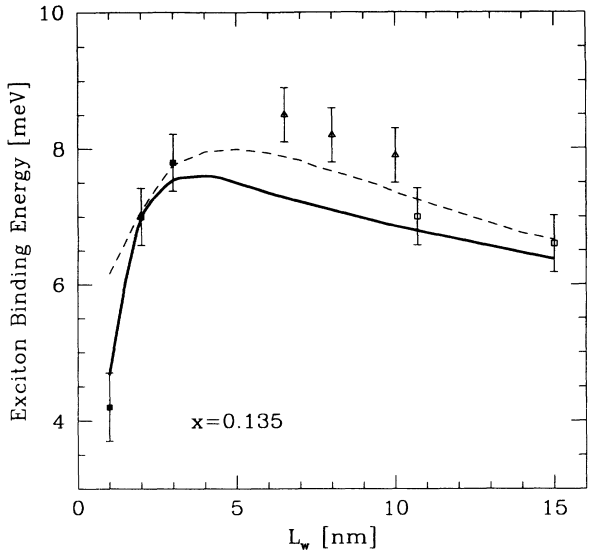

FIG. 5. Exciton binding energy as a function of the quantum well width L_w in the four-band model (solid line) and in the two-band model (dashed line). Theoretical results are given for an $In_xGa_{1-x}As$ quantum well with $x = 0.135$ and Q_v=0.45. Experimental results are shown for QW's with $x = 0.135$ [full squares (Ref. 7) and triangles (Ref. 3)] and $x = 0.13$ [open squares (Ref. 7)].

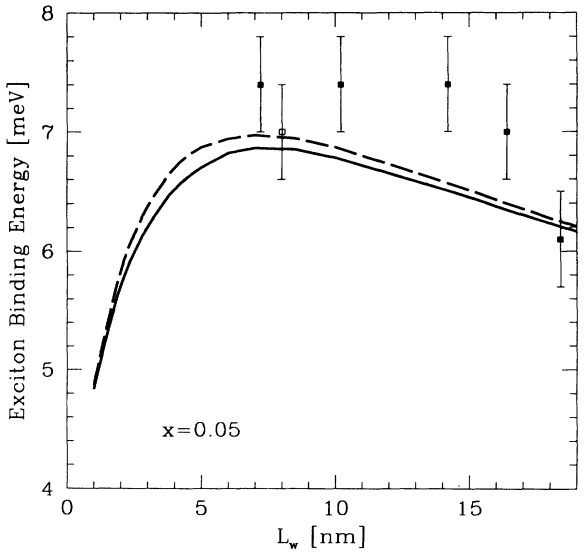

FIG. 4. Exciton binding energy as a function of the well width L_w. Theoretical curves are computed for an $In_xGa_{1-x}As$ quantum well with $x = 0.05$, and Q_v=0.45 (solid line) and Q_v=0.30 (dashed line). Experimental results are shown for QW's with $x = 0.05$ [full squares (Ref. 8)] and $x = 0.07$ [open square (Ref. 3)].

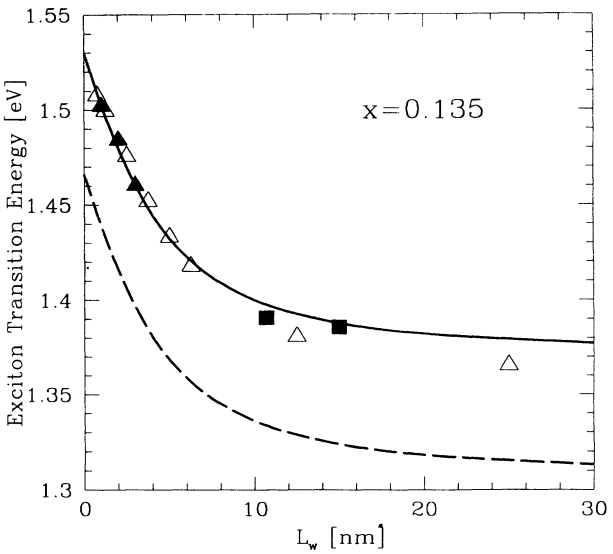

FIG. 6. Calculated absorption energy of the lowest heavy-hole exciton state as a function of the well width L_w in QW samples of $In_xGa_{1-x}As$ strained (solid curve) and unstrained (dashed curve). Experimental results are shown for $x = 0.13$ [full squares (Ref. 7)], $x = 0.135$ [full triangles (Ref. 7)], and $x = 0.14$ [empty triangles (Ref. 9)].

be due to a different evaluation of the continuum threshold, while the uncertainty between nominal and real parameter values of the samples has a minor role. It is also worthwhile to observe that the values for very small thicknesses ($L_w < 20$ Å) are computed on multiple QW's ($N > 7$) in the four-band model calculations.

To emphasize the role of strain effects we finally report in Fig. 6 the theoretical values and the experimental energies of the absorption peaks of the heavy-hole exciton as a function of well width for quantum wells with indium concentration $x = 0.135$ (Ref. 7). The theoretical exciton energies computed with the four-band model are shown for strained samples (solid curve) and for unstrained ones (dashed curve). The good agreement between theory and experiments underlines the validity of the model adopted for the calculation of the strain effects.

V. CONCLUSIONS

We would like summarize the results obtained above as follows.

Exciton variational calculations are carried out with different degrees of accuracy including the effect of internal strain by a virtual-crystal approach. This allows us to reproduce the heavy-hole exciton binding energies in $In_xGa_{1-x}As/GaAs$ strained materials without fitting parameters.

Results obtained with the four-band and the two-band model compare very well with a large set of experimental energies measured in samples with different well thicknesses and different indium concentrations. Multiple quantum well calculations of the optical response function give an excitation spectrum and a line shape structure in good agreement with experiment showing evidence for heavy-hole and light-hole excitons. The light-hole exciton is confined because of the electron attraction, while the light hole alone would be delocalized.

Exciton energies are well reproduced by the theory in a set of quantum wells with large indium concentration (about $x = 0.13$); this agreement is obtained for a set of samples grown in the same apparatus under the same conditions (Ref. 7), provided the heavy-hole band-offset value is in the range $Q_v = 0.30 - 0.45$.

ACKNOWLEDGMENTS

Two of the authors (A.D. and N.T.) are indebted to "Progetto Finalizzato Materiali Speciali per Tecnologie Avanzate" of the National Research Council of Italy for financial support.

[1] K. J. Moore, G. Duggan, K. Woodbridge, and C. Roberts, Phys. Rev. B **41**, 1090 (1990).
[2] G. Duggan, K. J. Moore, B. Samson, A. Raukema, and K. Woodbridge, Phys. Rev. **42**, 5142 (1990).
[3] H. Q. Hou, Y. Segawa, Y. Aoyagi, S. Namba, and J. M. Zhou, Phys. Rev. B **42**, 1284 (1990).
[4] B. Jogai and P. W. Yu, Phys. Rev. B **41**, 12 650 (1990).
[5] B. Gil, P. Lefebvre, P. Boring, K. J. Moore, G. Duggan, and K. Woodbridge, Phys. Rev. B **44**, 1942 (1991).
[6] D. C. Reynolds, K. R. Evans, C. E. Stutz, B. Jogai, C. R. Wie, and P. W. Yu, Phys. Rev. B **45**, 11 156 (1992).
[7] J. P. Reithmaier, R. Hoger, and H. Riechert, Phys. Rev. B **43**, 4933 (1991).
[8] M. J. Joyes, Z. Xu, and M. Gal, Phys. Rev. B **44**, 3144 (1991).
[9] W. Zhou, M. Dutta, D. D. Smith, J. Pamulapati, H. Shen, P. Newman, and R. Sacks, Phys. Rev. B **48**, 5256 (1993).
[10] J. Y. Marzin, in *Heterojunctions and Semiconductor Superlattices*, edited by G. Allan, G. Bastard, N. Boccara, M. Lannoo, and M. Voos (Springer-Verlag, Berlin, 1985).
[11] J. Y. Marzin, M. N. Charasse, and B. Sermage, Phys. Rev. B **31**, 8298 (1985).
[12] J. M. Luttinger and W. Kohn, Phys. Rev. **97**, 869 (1955); J. M. Luttinger, *ibid.* **102**, 1030 (1956).
[13] G. L. Bir and G. E. Pikus, *Symmetry and Strain-Induced Effects in Semiconductors* (John Wiley, New York, 1974).
[14] L. Laude, F. H. Pollak, and M. Cardona, Phys. Rev. B **3**, 2623 (1971).
[15] F. H. Pollak, in *Semiconductors and Semimetals*, edited by T. P. Paersel (Academic, New York, 1990), Vol. 32.
[16] S. Adachi, J. Appl. Phys. **53**, 8775 (1982).
[17] G. Bastard, *Wave Mechanics Applied to Semiconductor Structures* (Les Editions de Physique CNRS, Paris, 1988).
[18] M. G. Burt, J. Phys. Condens. Matter **4**, 6651 (1992).
[19] A. D'Andrea and R. Del Sole, Phys. Rev. B **41**, 1413 (1990).
[20] A. D'Andrea and N. Tomassini, Phys. Rev. B **47**, 7176 (1993).
[21] *Semiconductors. Physics of Group IV Elements and III-V Compounds*, edited by O. Madelung, Landolt-Börnstein, New Series, Group III, Vol. 17, Pt. a (Springer, Berlin, 1982).
[22] R. Atanasov and F. Bassani, Solid State Commun. **84**, 71 (1992).
[23] R. Atanasov, F. Bassani, and V. M. Agranovich, Phys. Rev. B **49**, 2658 (1994).
[24] S. Fraizzoli, F. Bassani, and R. Buczko, Phys. Rev. B **41**, 5096 (1990).